Pressure pulsation during the outlet pressure variation process of the pump turbine under operating conditions

Zhenggui Li[1,2*], Lixin Xu[2], Wangxu Li[3], Chuanshi Cheng[4], Xiaotong Song[1], Yanxiong Jiao[1], Dongbing Jin[5], Meiying San[5]

(1. *School of Engineering, Qinghai Institute of Technology, Xining, Qinghai 810016, China*;
2. *Key Laboratory of Fluid and Power Machinery of the Ministry of Education, Xihua University, Chengdu 610039, China*;
3. *School of Energy and Power Engineering, Lanzhou University of Technology, Lanzhou 730050, China*;
4. *Changjiang Electric Power Co., Ltd, Yichang 443002, Hubei, China*;
5. *Huanghe Hydropower Development Co., Ltd, Xining 810008, China*)

Abstract: This paper studies the flow characteristics of the pump turbine of a pump under operating conditions during the outlet pressure variation process, aiming to improve its operational stability in pumping and compressing air energy storage systems. Through numerical simulations of the flow process, the pressure distribution and pressure pulsation characteristics in key areas such as the volute, double-row impeller, runner, and tailpipe are analyzed in depth. The study reveals that during the outlet pressure variation process under operating conditions, the pressure distribution is directly influenced by the outlet pressure variation, while pressure pulsation is mainly affected by the dynamic and static interference within the unit, with the pressure pulsation amplitude influenced by the rate of pressure variation. The results indicate that during the outlet pressure variation process, it is important to prevent the outlet pressure from staying in unstable working ranges to reduce the intensity of pressure pulsation. A smoother rate of pressure variation should be adopted before stopping the outlet pressure variation to reduce the "pressure variation inertia" and enhance the overall operational stability of the water turbine unit.

Keywords: pump turbine, outlet pressure variation, pressure pulsation, numerical simulation
DOI: 10.25165/j.ijabe.20251802.9266

Citation: Li Z G, Xu L X, Li W X, Cheng C S, Song X T, Jiao Y X, et al. Pressure pulsation during the outlet pressure variation process of the pump turbine under operating conditions. Int J Agric & Biol Eng, 2025; 18(2): 155–164.

1 Introduction

With the rapid development of modern hydropower technology, the pump turbine, as an important hydroelectric equipment, has garnered wide attention regarding its operational efficiency and safety[1-4]. Particularly, the pressure pulsation behavior under operating conditions challenges the overall stability of the unit. Some researchers have attempted to address stability issues at the device level[5-8], but unpredictable pressure pulsations still pose a significant potential hazard. A thorough understanding of the pressure pulsation characteristics of the pump turbine under operating conditions can contribute to further enhancing the efficiency and stability of the unit.

In recent years, research on the pressure pulsation characteristics of internal flow fields in non-optimal conditions of water turbines has become a hot topic. Oscillatory damping phenomena under unsteady states of low specific speed water turbines have been discovered[9], and there is a new understanding of the effects and interaction mechanisms of internal pressure pulsations on dynamic stress characteristics under extreme head conditions[10]. Li Qifei et al.[11] analyzed the transitional process of the active guide vanes of water turbine units at small opening angles, deeply investigating the flow field structure in the guide vane area and the variations in pressure pulsations in that region. Compared to non-optimal conditions, structural vibration issues are more likely during operation transitions, necessitating particular attention to pressure pulsations during transient processes. Kim et al.[12] studied the internal flow phenomena corresponding to different values of the Thoma number in a pump turbine model under turbine operation, finding that low Thoma numbers significantly enhance irregular flow along the flow direction, thereby exacerbating unsteady pressure pulsations. Yin et al.[13] conducted numerical studies on the flow and structural characteristics during the start-up process of large high-head pump turbines, revealing that increased component pressures and intensified internal flow under turbine operation lead to exacerbated pressure pulsations, causing stress concentration that affects system stability. Zhang et al.[14] found in their numerical study of transient exhaust pressurization of pump turbines that in addition to the main frequency being the blade passing frequency and its harmonic frequencies, high-amplitude bands caused by flow detachment and centrifugal effects are also present in this area.

In summary, research on the pressure pulsation characteristics of pump turbines has progressed from surface to mechanistic investigations. However, there is still not a comprehensive understanding of the pressure pulsation characteristics during the outlet

Received date: 2024-07-31 **Accepted date:** 2025-01-09
Biographies: Lixin Xu, research interest: internal flow and stability of hydraulic machinery, Email: 1083670127@qq.com; **Wangxu Li**, research interest: magnetic liquid sealing technology, Email: 1121076860@qq.com; **Chuanshi Cheng**, research interest: internal flow and stability of hydraulic machinery, Email: 212023085800027@stu.xhu.edu.cn; **Xiaotong Song**, research interest: internal flow and stability of hydraulic machinery, Email: xtsong@qhit.edu.cn; **Yanxiong Jiao**, research interest: internal flow and stability of hydraulic machinery, Email: yxjiao@qhit.edu.cn; **Dongbing Jin**, research interest: internal flow and stability of hydraulic machinery, Email: 1795439078@qq.com; **Meiying San**, research interest: internal flow and stability of hydraulic machinery, Email: 1552292075@qq.com.
***Corresponding author: Zhenggui Li**, Professor, research interest: magnetic liquid sealing technology. Qinghai Institute of Technology, Xining, 810016, China. Tel: +86-17602832345, Email: lzhgui@mail.xhu.edu.cn.

pressure variation process under operating conditions. In studying the pressure pulsation characteristics of pump turbines, model experimental research faces limitations such as high costs, numerous equipment restrictions, difficulties in displaying flow fields, and lengthy processing times. With the development of computer and image processing technologies, numerical simulations have become a critical tool for studying complex flow fields[15-19]. This paper employs numerical simulation methods to explore the internal flow characteristics of pump turbines under operating conditions, delving into the impact of the outlet pressure variation process on pressure pulsations in the volute, double-row impeller domain, runner domain, and tailpipe domain. By detailed comparisons of pressure pulsations within different pressure variation conditions, the dynamic evolution mechanisms of the internal flow regime are revealed. This study offers new insights and methods for the design, operation, and optimization of pump turbines.

2 Calculation model and numerical computation method

2.1 Model parameters

To investigate the outlet pressure variation process of the pump turbine, this paper takes a certain prototype machine of a pump turbine as the basis, mainly involving the volute, double-row impeller domain, runner domain, and tailpipe domain. The main design parameters of the model are listed in Table 1.

The components of the unit were modeled in three dimensions using UG NX software, with the entire flow area inside the pump turbine unit serving as the computational domain. The assembled components form the overall model as shown in Figure 1.

2.2 Grid division

Due to the complexity of the flow characteristics of pump turbines and the precision requirements for calculations, this paper employs a structured grid partitioning method to achieve accurate grid division of the pump turbine model. Prior to numerical computation, five different grid configurations were utilized, each containing grid numbers ranging from 2.3 million to 6.9 million. These configurations were compared and validated using optimal operating parameters during pump conditions. The aim was to ensure the stability and reliability of the simulation results through a comprehensive comparative analysis[20-24]. The grid model with 6.1 million grid cells was selected for this calculation, as shown in Figure 2.

Table 1 Basic parameters of model pump turbine

Argument	Value	Argument	Value
Runner inlet diameter D_1/mm	3820	Number of fixed guide vanes	20
Runner outlet diameter D_2/mm	2920	Number of active guide blades	20
Number of runner blades	9	Guide vane opening, °	20.5

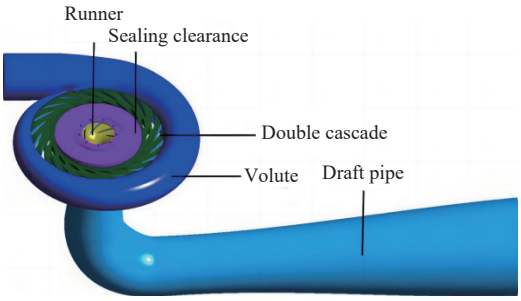

Figure 1 3D model of pump turbine

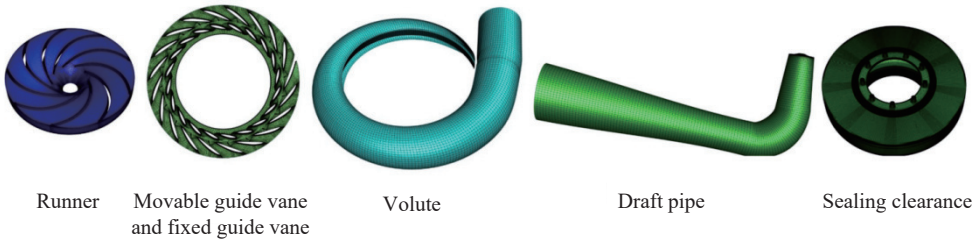

Figure 2 Region grid of each part

2.3 Fluid control equation

This paper mainly investigates the pressure pulsation characteristics during the outlet pressure variation process of the pump turbine under operating conditions. The SST k-ω turbulence model combines the SST k-ω and k-ε models to accurately predict flow phenomena over a wide range. By utilizing blending functions for numerical solutions in different regions, this model can effectively capture flow separation and vortex shedding phenomena within the boundary layer[25-29]. Therefore, this paper adopts the SST k-ω turbulence model for simulation calculations.

The mathematical expressions for the SST k-ω turbulence model are represented by Equations 1 and 2:

$$\frac{\partial}{\partial x_i}(\rho k u_i) = \frac{\partial}{\partial x_i}\left(\Gamma_k \frac{\partial k}{\partial x_j}\right) + \overline{G_k} - Y_k + S_k \quad (1)$$

$$\frac{\partial}{\partial x_i}(\rho \omega u_i) = \frac{\partial}{\partial x_i}\left(\Gamma_\omega \frac{\partial \omega}{\partial x_j}\right) + G_\omega - Y_\omega + D_\omega + S_\omega \quad (2)$$

where, k represents turbulent kinetic energy; ω denotes turbulent dissipation rate; $\overline{G_k}$ and G_ω signify the generation terms for turbulent kinetic energy and dissipation rate; Γ_k and Γ_ω are the effective diffusion terms for turbulent kinetic energy and dissipation rate; Y_k and Y_ω correspond to the dissipation terms for turbulent kinetic energy and dissipation rate; D_ω indicates the orthogonal diffusion term, while S_k and S_ω represent the source terms for turbulent kinetic energy and dissipation rate.

2.4 Initial values and boundary conditions

Taking into account the system's outlet pressure variations and the unit's external characteristics, assuming the outlet pressure at optimal operating conditions as P_{BET}, this paper designs eight different outlet pressure change scenarios to simulate various outlet pressure variation processes. Each scenario corresponds to a different pressure change rate. Specifically, four scenarios (P1, P2, P7, P8) have outlet pressure changes gradually transitioning from 1.1 times the outlet pressure at optimal conditions ($P_{1.1BET}$) to P_{BET}, while the other four scenarios (P3, P4, P5, P6) involve outlet pressure changes transitioning from 1.1 times the outlet pressure at optimal conditions ($P_{1.1BET}$) to 0.9 times the outlet pressure at optimal conditions ($P_{0.9BET}$). The outlet pressure variation conditions are illustrated in Figure 3, where (t_0) denotes the start time of pressure variation, and (t_{20}) and (t_{30}) represent the stop times of pressure variation (subscripts indicating the number of runner rotations after the start of pressure variation).

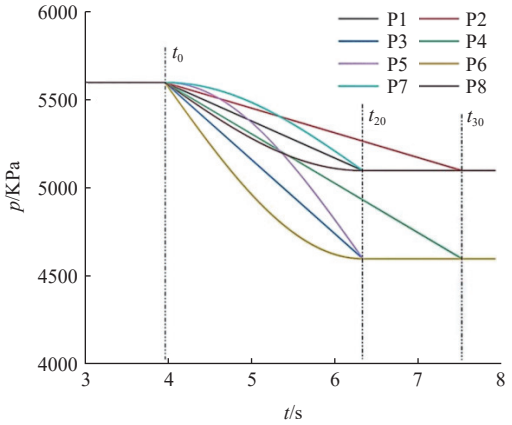

Figure 3 Variations in outlet pressure

To study the changes in outlet pressure during pump conditions, the outlet of the tailpipe is chosen as the inlet boundary. Water flows from the tailpipe into the model with the flow direction perpendicular to the inlet surface. The volute is selected as the outlet boundary, and the outlet pressure is input using a custom formula from text data. The model wall surfaces are set with no-slip boundary conditions, while connections between components such as the volute, guide vane, runner, and tailpipe are established using Interfaces. The numerical solution of the governing equations is conducted using the SIMPLEC algorithm, with a turbulence intensity I set at 5%. Additionally, the steady-state results serve as the initial field for transient simulation calculations of the pressure variation process. The computational time step is defined as the time corresponding to a one-degree rotation of the runner, with a maximum iteration number of 80.

2.5 Verification of simulation accuracy

The full characteristic curve of a pump or a turbine exhibits an "S"-shaped curve in the operating region. Hence, this region is referred to as the "S-characteristic curve" for the water turbine. In order to ensure the accuracy of the simulation results for the outlet pressure variation operation, this paper numerically simulated the computational external characteristics of this model under 20 different flow conditions. It compared and analyzed the computed external characteristic curves with the measured external characteristic curves of the prototype machine. The results are shown in Figure 4.

From the graph, it is evident that the computed curve closely follows the trend of the measured data. In the H-Q curve plot, there is a noticeable peak phenomenon when the flow rate ranges between 40-50 m^3/s. The measured and simulated values within this range exhibit high consistency, with errors strictly controlled within 1%. As the flow rate moves away from this interval, the errors fall within the range of 1% to 4%. In the η-Q curve plot, the error trends show a decrease followed by an increase with increasing flow rates. Even at maximum and minimum flow rates, the maximum error is only 4.84%. Overall, the model's calculation results maintain errors well below 5%, validating the accuracy and reliability of the model in simulating the operational state of the pump turbine under pump conditions.

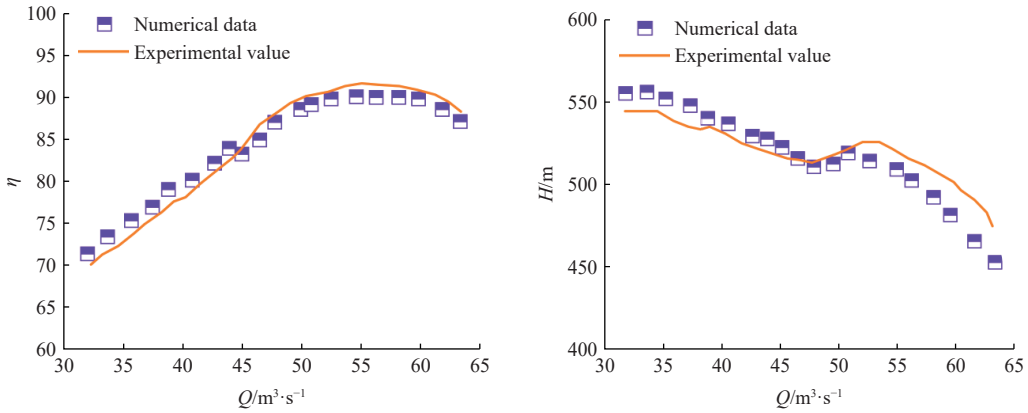

Figure 4 Comparison of model and prototype external characteristics

3 Analysis of steady-state flow field numerical results

This paper conducts a time-domain analysis of pressure monitoring points in areas such as the volute, double-row impeller, runner, and tailpipe, aiming to study the temporal changes in pressure, as well as the amplitude and frequency characteristics of pressure pulsations. For the pressure pulsation monitoring data in the runner area after the cessation of outlet pressure variation, Fast Fourier Transform (FFT) is used to perform frequency domain analysis on the pressure pulsation signals, identifying the primary frequency components and corresponding vibration modes. Furthermore, this paper also comparatively studies the effect of outlet pressure change rates under pump conditions on the internal pressure pulsations of the pump turbine.

3.1 Pressure distribution in the volute region

Figure 5 shows the pressure distribution in the volute under different operating conditions. From the graph, it is evident that the pressure on the inner side of the volute (closer to the double-row impeller side) is significantly higher than on the outer side (far from the double-row impeller side), with the most noticeable pressure difference between the inner and outer sides occurring at the front end of the volute tongue. This indicates that within the volute, the fluid is influenced by the guide vanes, leading to higher velocities on the inner side resulting in lower pressure, while the wider flow path on the outer side causes slower velocities and relatively higher pressure.

There is a noticeable localized pressure concentration phenomenon in the region where the volute meets the double-row impeller. These concentrated areas of relatively high pressure correspond directly to the positions of the fixed guide vanes. Between every two adjacent regions of relatively high pressure, there exists a region of relatively low pressure, and the position of this low-pressure region aligns precisely with the internal flow passage of the double-row impeller. The formation of these high- and low-pressure regions is closely related to the fluid flow characteristics, as fluid directly enters the channel at a higher

velocity in the area adjacent to the double-row impeller passages, while in the region neighboring the fixed guide vanes, the fluid slowdown results in an increase in static pressure.

During the outlet pressure variation process, as the outlet pressure gradually decreases, the pressure within the volute region also shows a corresponding decreasing trend. However, the rate of change of the outlet pressure affects the magnitude of the pressure variations within the volute region. A comparison between scenarios P1 and P2 reveals that under conditions where the outlet pressure values are equal (the outlet pressure at time (t_{10}) in scenario P1 is the same as the outlet pressure at time (t_{15}) in scenario P2), the higher the outlet pressure change rate, the higher the overall pressure in the volute region. Similar phenomena are observed when comparing scenarios P3 and P4, P5 and P6, as well as P7 and P8, further confirming the relationship between the outlet pressure change rate and the internal pressure variations within the volute region.

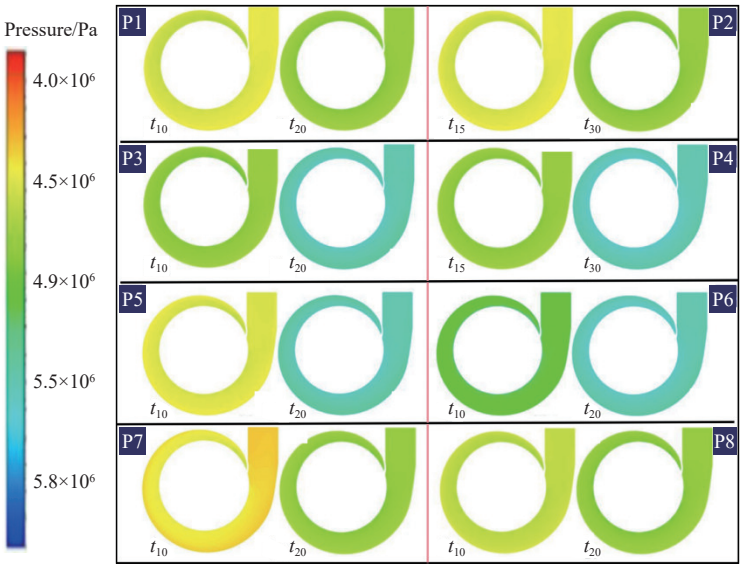

Figure 5 Comparison of model and prototype external characteristics

3.2 Pressure distribution in double-row cascade area

In pump conditions, the flow of water in the double-row impeller region passes through the movable guide vanes, fixed guide vanes, and finally flows into the volute from the runner area. Figure 6 shows the pressure distribution in the double-row impeller region under different operating conditions. From the graph, it can be seen that the pressure distribution in the double-row impeller region exhibits a decreasing trend. Starting from the boundary with the volute, passing through the area of the fixed guide vanes, the region of the movable guide vanes, and finally reaching the runner area, the pressure values gradually decrease.

The localized high-pressure areas in the double-row impeller region are mainly concentrated at the front end of the movable guide vanes (far from the side of the fixed guide vanes), while the localized low-pressure zones are primarily concentrated at the rear end of the movable guide vanes (near the side of the fixed guide vanes). Pressure fluctuations appear near the volute tongue, specifically on the outer side of the double-row impeller region (far from the runner area) corresponding to the same circumference area as the inner side of the volute. Pressure gradually increases from the volute tongue end towards the exit of the volute passage. Near the inner side of the double-row impeller region (closer to the runner area), the pressure values are higher near the front end of the volute tongue.

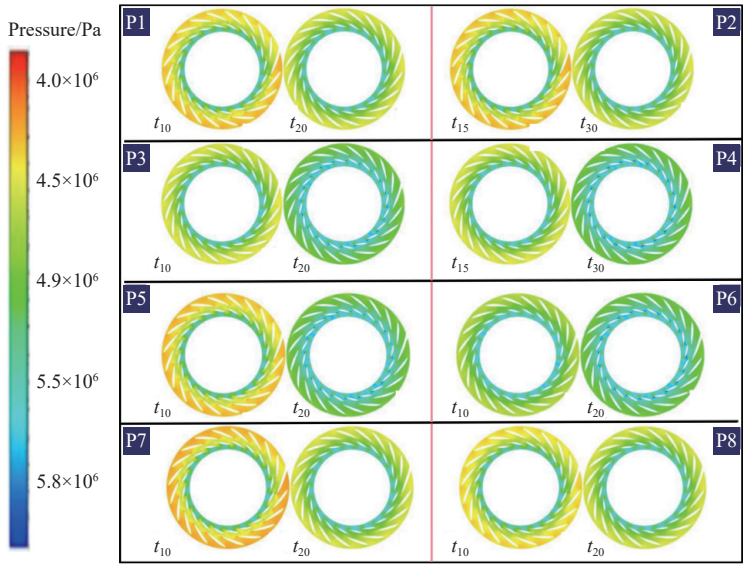

Figure 6 Pressure distribution of double-row cascade

Under the outlet pressure variation conditions, as the outlet pressure gradually decreases, the pressure within the double-row impeller region also shows a corresponding decreasing trend, with the area of localized low pressure at the rear end of the movable guide vanes gradually increasing. However, the rate of change of the outlet pressure affects the magnitude of pressure variations within the double-row impeller region. A comparison between scenarios P1 and P2 reveals that under conditions where the outlet pressure values are equal (the outlet pressure at time (t_{10}) in scenario P1 is the same as the outlet pressure at time (t_{15}) in scenario P2), the higher the outlet pressure change rate, the lower the overall pressure in the double-row impeller region. Similar phenomena are validated when comparing scenarios P3 and P4, P5 and P6, as well as P7 and P8.

In this operating condition, the overall pressure distribution within the double-row impeller region is directly influenced by the outlet pressure change rate and the amplitude of the outlet pressure, but considering the influence of incoming flow in the runner area, the overall pressure change magnitude in this region is slightly smaller compared to the volute region.

3.3 Pressure distribution in the runner region

In the operating condition of a pump, water flows from the tailwater pipe into the impeller region. The pressure on the mid-surface of the impeller gradually increases in the direction of the flow, forming a low-pressure zone on the suction side of the blade (the concave surface) and a high-pressure zone on the pressure side (the convex surface) of the blade. Figure 7 illustrates the pressure distribution on the mid-surface of the impeller region during the pressure variation process. It can be seen from the figure that the overall low-pressure zone within the flow channel is concentrated at the inlet side, while a localized high-pressure zone is formed at the top of the impeller blades due to the impact of the water flow. At the same time, the trailing edge of the impeller blades exhibits a coexistence of localized high-pressure and corresponding localized low-pressure zones. This phenomenon is attributed to the flow separation at the trailing edge during the rotation of the blades and the dynamic changes in pressure difference at the interface of both sides of the blades, leading to instability in the flow state within the flow channel.

During the outlet pressure variation process, when the outlet pressure variation occurs more rapidly, the overall pressure within the impeller region becomes lower, and the amplitude of pressure variation at the outlet end of the impeller flow channel is greater than that at the low-pressure inlet end. A comparison between conditions P1 and P2 shows that under the condition of equal outlet pressure values (the outlet pressure at time (t_{10}) for condition P1 is equal to the outlet pressure at time (t_{15}) for condition P2), the higher the rate of outlet pressure variation, the lower the overall pressure within the impeller region. A similar phenomenon is also verified in the comparison of conditions P3 and P4, P5 and P6, and P7 and P8.

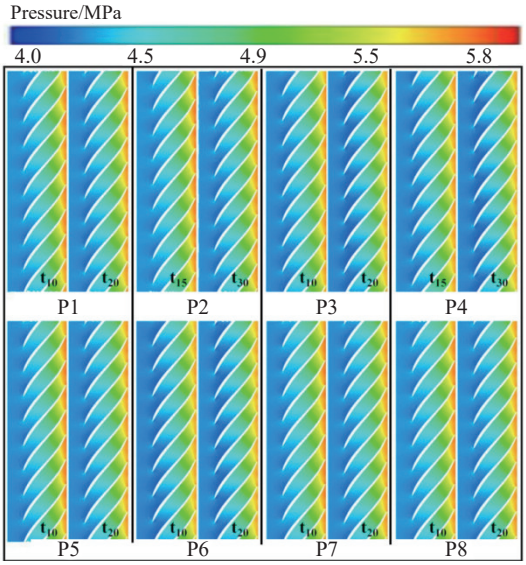

Figure 7 Pressure distribution of runner

3.4 Pressure distribution in the draft pipe area

Under the operating condition of a pump, water flows from the tailwater pipe inlet, passing through the tailwater pipe channel into the impeller region. Figure 8 shows the pressure distribution in the tailwater pipe during the pressure variation process. From the figure, it can be observed that the end of the tailwater pipe near the impeller region presents a low-pressure zone, with a relatively high-pressure zone located at the center of the pipe within this low-pressure area. Additionally, the outer side of the bend in the tailwater pipe exhibits a relatively high-pressure zone, while the inner side forms a relatively low-pressure zone, indicating that the bend structure significantly affects the pressure distribution. In the downstream section of the bend, the pressure increases gradually in the direction of the water flow.

During the outlet pressure variation process, the area of the low-pressure zone at the outlet end of the tailwater pipe gradually increases, while the high-pressure area on the outer side of the bend

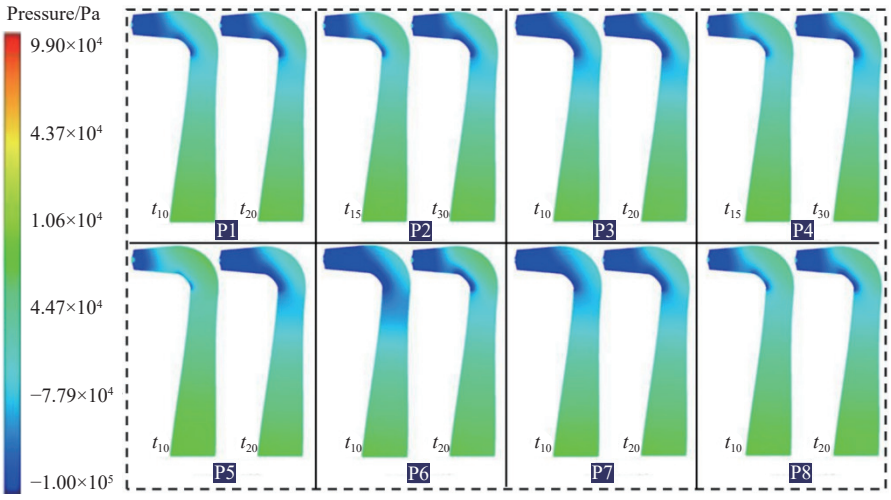

Figure 8 Pressure distribution of tailpipe

decreases and the low-pressure area on the inner side increases, directly affecting the magnitude and distribution of pressure within the tailwater pipe. A comparison between conditions P1 and P2 shows that under the condition of equal outlet pressure values (the outlet pressure at time (t_{10}) for condition P1 is the same as the outlet pressure at time (t_{15}) for condition P2), the higher the rate of outlet pressure variation, the larger the area of the low-pressure zone at the outlet end of the tailwater pipe, the smaller the high-pressure area on the outer side of the bend, and the larger the low-pressure area on the inner side. A similar phenomenon is also confirmed in the comparison of conditions P3 and P4, P5 and P6, and P7 and P8.

4 Transient flow field pressure pulsation analysis

4.1 Pressure pulsation monitoring point settings

To study the pressure pulsation characteristics inside the model during the outlet pressure variation process, it is necessary to set multiple monitoring points at different locations within the model. When selecting monitoring points, two main principles are typically followed: the primary principle ensures that the monitoring points accurately reflect the pulsation characteristics of the flow components, and the secondary principle ensures observability across various simulation methods.

In this study, a total of 34 pressure pulsation monitoring points were set in areas including the volute, double-row impeller region, vaneless area, runner, and draft tube. The starting time of the pressure variation process was taken as the baseline time point for analyzing the pressure pulsation at these monitoring points. The specific layout is shown in Figure 9. In the volute section, seven monitoring points were sequentially established, named SC1 to SC7. In the fixed guide vane channel, the area where fixed guide vanes meet movable guide vanes, and the region of the movable guide vanes, a total of twelve monitoring points were arranged, named SY1-1 to SY4-3. In the runner area, three monitoring points were set along the pressure surface, named RN4 to RN6, and three monitoring points were also set along the suction surface, named RN1 to RN3. Finally, in the draft tube area, nine monitoring points were placed along the straight cone and diffuser section SW1, SW2, and SW3 interfaces, named SW1-1 to SW3-3.

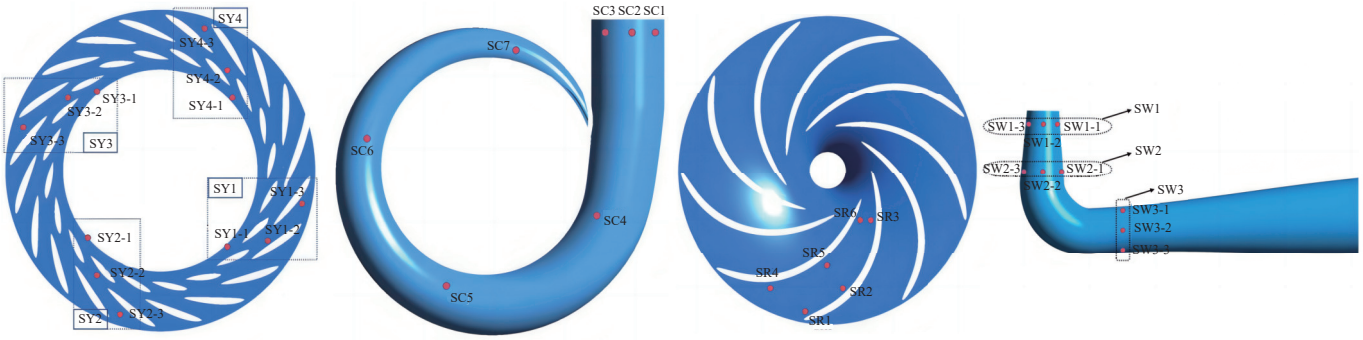

Figure 9 Pressure pulsation monitoring points

Pressure pulsation analysis methods mainly focus on two aspects: time domain analysis and frequency domain analysis. Time domain analysis primarily explores the dynamic changes in pressure magnitude over time. Frequency domain analysis treats discrete data as an integration of periodic and random signals, commonly using Fast Fourier Transform (FFT) to transform time-domain data into frequency-domain data for effective processing of parts that are difficult to handle directly in the time domain.

To represent the changing patterns and relationships of pressure pulsations at internal measurement points within hydroelectric pump-turbines more clearly, this study conducts both time domain and frequency domain analyses using the Fast Fourier Analysis method. The rotational speed of the runner f_n is $n/60$ = 20 Hz, and the number of blades in the runner Z is 9. The non-dimensional pressure pulsation coefficient C_P is used to characterize the intensity of pressure pulsations. The formula is given by[5]:

$$C_P = \frac{P_i - \bar{P}_i}{P_{BET}} \quad (3)$$

where, P_i is the pressure at point i, Pa; $\bar{P}_i$ is the pressure at point i after being smoothed using the LOSS method, Pa; and P_{BEP} is the outlet pressure at the optimal operational state of the machine, Pa.

4.2 Pressure pulsation in the volute area

In Figure 10, the pressure and pressure pulsation spectrogram of monitoring points in the volute region are shown. From the graph, it can be observed that when the outlet pressure stabilizes at $P_{1.1BEP}$, the pressure values at monitoring points SC1, SC2, and SC3 at the volute outlet are close, exhibiting a consistent decreasing trend with the decrease in outlet pressure, resulting in a relatively small overall pulsation coefficient. As the monitoring points move deeper into the volute, the pressure values gradually decrease from SC1 to SC7. Particularly at monitoring point SC7 near the tongue, the pressure pulsation becomes more significant due to the influence of unstable flow entering from the double-row impeller region. Overall, the maximum average pressure difference between monitoring points reaches 92.3 kPa, indicating a notable pressure gradient within the volute.

In the process of variable pressure, the change of outlet pressure will directly lead to the increase of adverse flow. Especially in the initial stage of the pressure fluctuation, the pressure fluctuation coefficient will increase greatly, forming a high amplitude area of pressure fluctuation. For example, at P3, the SC6 reaches its maximum pressure ripple coefficient at 0.798 s. This region of high amplitude coincides with the time point of the high vortex area inside the volute shown in Figure 5. It should be noted that after the high-amplitude area, the pressure variation of SC6 will decrease before other working conditions.

For different outlet transformer conditions, such as transformer to P_{BEP} and $P_{0.9BEP}$, the fluctuation coefficient varies. The former will decrease after a large increase, and the maximum difference of average pressure after stability is 60.1 kPa. The latter decreased after the surge amplitude increased significantly, but then continued to increase. After the surge pressure stops, the maximum difference of average pressure is 90.5 kPa, accompanied by an obvious cyclical fluctuation peak.

The above phenomenon shows that the pressure pulsation in the

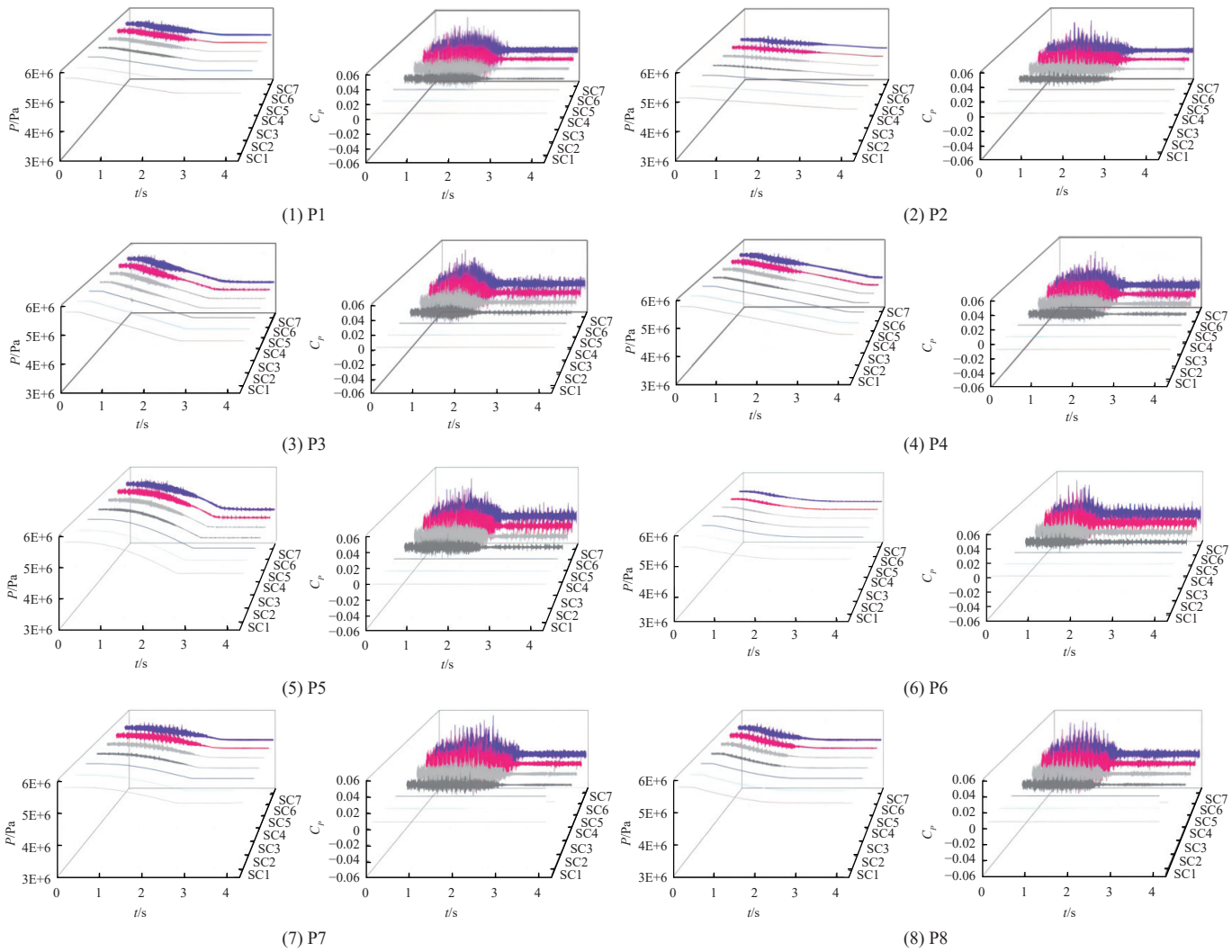

Figure 10 Time domain diagram of volute pressure pulsation

volute region is directly affected by the separation of fluid flow in the upstream basin and the change of outlet pressure. When the outlet pressure changes from $P_{1.1BEP}$ to P_{BEP}, the unstable flow in the double-row cascade region increases and decreases, which leads to the weakening of the momentum conversion energy in the volute region and strengthens the transmission of undesirable pulsations in the double-row cascade region. In view of this, the faster outlet pressure change is conducive to reducing the maximum ripple coefficient in the volute region, thus enhancing the stability of the unit.

4.3 Pressure pulsation in the runner area

After the outlet pressure stops changing, the flow state within the volute region requires a period of adjustment to reach a relatively stable state. This phenomenon of delayed flow adjustment primarily originates from the runner region. Under changing pressure conditions, understanding the patterns and magnitudes of pressure pulsations in the runner region is crucial for comprehending the flow state within the volute.

In order to quantitatively characterize the intensity of pressure pulsations in the runner region, this study introduces the dimensionless pressure pulsation coefficient C_{P1}, expressed as[5]:

$$C_{P1} = \frac{P_i - \bar{P}}{P_{out}} \tag{4}$$

where, P_i is the pressure at point i, Pa; $\bar{P}$ is the average pressure, Pa; P_{out} is the outlet pressure, Pa.

From Figures 6 and 7, it is evident that there are two high-pressure regions and two low-pressure regions within the vaneless area. During the rotation of the runner, the blades periodically pass through these high and low-pressure zones within the volute. As the runner blades rotate, they cyclically move through these high- and low-pressure areas, leading to periodic variations in the amplitude of the time-domain signals at monitoring points. The signal reaches its maximum amplitude in the high-pressure region and drops to the minimum in the low-pressure region. This variation creates a cyclical signal, generating nine high peaks after one rotation of the runner, corresponding to the number of blades.

Analysis from Figure 11 reveals that under various pressure changing conditions, the amplitude of pressure pulsations decreases gradually from the outlet to the inlet of the runner in the time-domain signals. Additionally, the pressure pulsation intensity on the suction side of the blades is significantly greater than that on the corresponding pressure side. Influenced by the periodic disturbance of the blades, the main frequency at each measurement point is 18.00 fn while the sub-frequency is 9.00 fn. Furthermore, a series of frequency components can be observed such as 27.00 fn, 36.00 fn, 45.00 fn, all multiples of the number of runner blades, reflecting the phenomenon of equal harmonics. This occurrence is typically caused by the nonlinear interaction among different characteristic frequencies during pump and turbine operation conditions.

In the designated monitoring points of this study, initially, the maximum main frequency C_{P1} occurs at the suction side RN1-1 with values ranging from 0.082 39 to 0.088 36 under different

conditions. When the outlet pressure stabilizes at the $P_{0.9BEP}$ condition, the main frequency amplitude increases significantly, accompanied by the appearance of a sub-frequency at 0.5fn due to low-frequency high-amplitude surging inside the runner. After the outlet pressure stabilizes, although the low-amplitude pulsations across all frequencies decrease slightly, the amplitudes of the main frequency and the various blade multiple sub-frequencies increase. Additionally, the faster outlet pressure changing rates of conditions P6 and P7 generate more low-frequency pulsations in the initial stage of pressure stopping, mainly induced by vortices within the runner channels and swirl bands in the tailwater pipe area, but their impact is much smaller compared to the runner disturbances.

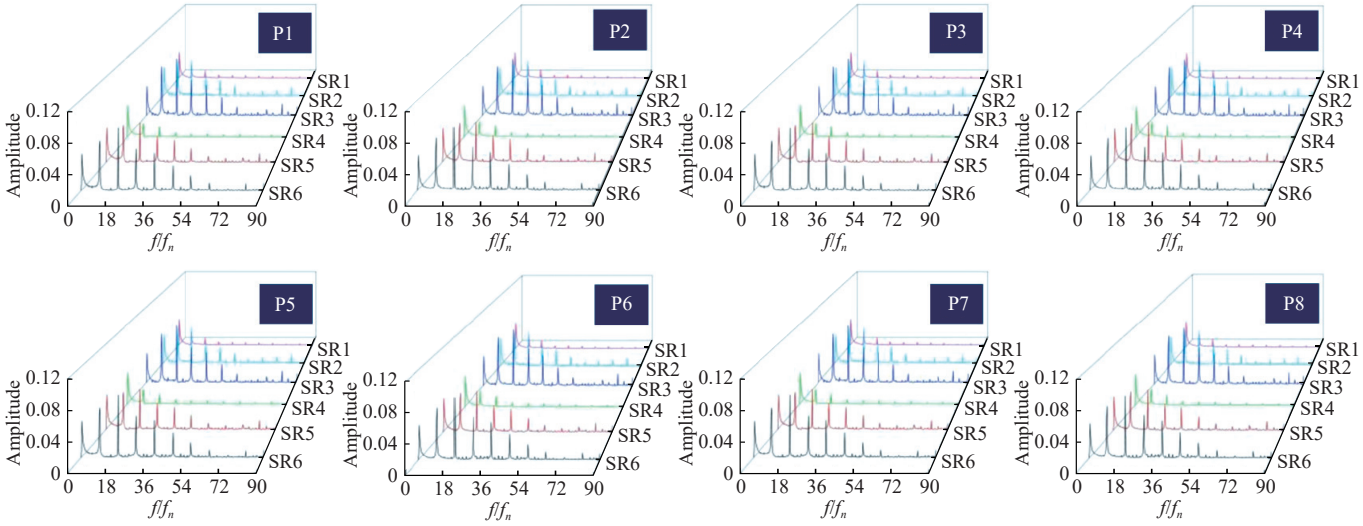

Figure 11 Frequency domain diagram of runner pressure pulsation

In conclusion, the pressure pulsations in the runner area have a significant impact on the flow state within the volute region. Their variation patterns are closely related not only to the rotation of the runner and the periodic disturbances caused by the blades but also influenced by various factors like the speed of outlet pressure changes. Hence, in practical applications, it is crucial to consider these factors comprehensively to achieve effective control over the flow state within the volute region.

4.4 Pressure pulsation in the draft pipe area

During the operation of a pump or turbine, the draft tube generates water pressure pulsations at different frequencies, which can lead to vibrations in the unit. From Figure 12, it can be observed that under the initial outlet pressure $P_{1.1BEP}$, no backflow is observed at the outlet of the draft tube. However, vortices are present at the SW1 section, and secondary flows caused by the rotation of the runner are detected near the wall surface. At this point, the pressures at SW1-1 and SW1-3 are both –142.28 kPa with a high C_P value of 0.021, while SW1-2 has a pressure of –65.1 kPa.

Along the draft tube from outlet to inlet, the pressures at SW2 and SW3 gradually increase, while the pressure pulsation coefficients decrease successively to 0.007. During the outlet pressure changing process, the amplitude of C_P change increases initially at various monitoring points in the draft tube and then decreases. Particularly, the C_P in the SW3 region starts decreasing before the SW2 and SW1 sections at 1.70 s. After the pressure changing stops, the pressure pulsations at the monitoring points exhibit periodic variations.

For the pressure changing conditions from outlet pressure to P_{BEP} like P1, P2, P7, and P8 conditions, the pressures at the draft tube monitoring points initially decrease and then increase during the pressure changing process, eventually stabilizing. The amplitude of the pressure changing decreases significantly after a large increase, and after stabilization, the maximum C_P at monitoring points near the wall surface on the SW1 section is less than 0.014, significantly higher than other monitoring points.

Under similar conditions from outlet pressure to $P_{0.9BEP}$, after the pressure changing stops, the maximum C_P of pressure pulsations at monitoring points is less than 0.015, and the maximum C_P value at the SW1 section is doubled compared to the SW2 section.

Further analysis reveals that the minimum C_P at the SW1 section occurs in the P6 condition, less than 0.036. The maximum pressure pulsation coefficients at SW1-1 and SW1-2 occur in the P2 and P7 conditions, respectively. The minimum and maximum C_P values at the SW2 and SW3 sections appear in the P6 and P2 conditions, respectively. After the pressure changing stops, the pressures at the draft tube monitoring points first increase and then stabilize, with the P2 condition requiring the longest time (0.396 s) and the P6 condition requiring the shortest time (0.044 s).

In conclusion, the outlet pressure changing rate affects the strength of backflow in the runner region and the distribution of secondary flow near the draft tube walls, thereby influencing the intensity of pressure pulsations in the draft tube area. Faster pressure changing rates can reduce the impact of the complex flow field within the runner area on the upstream draft tube. Therefore, in practical operations, controlling the pressure changing rate is an effective means to reduce unit vibrations and pressure pulsations in the draft tube.

5 Conclusions

1) Impact of outlet pressure changes on pressure distribution: Outlet pressure changes directly affect the pressure distribution within the system, with the degree of influence varying depending on the proximity to the runner region—the closer the distance, the weaker the impact. Pressure changes exhibit inertia throughout the system, meaning that the response of pressure is not instantaneous. The flow state in the runner region will alter due to outlet pressure changes, and this alteration will propagate to other parts of the system, subsequently affecting the pressure distribution in those areas.

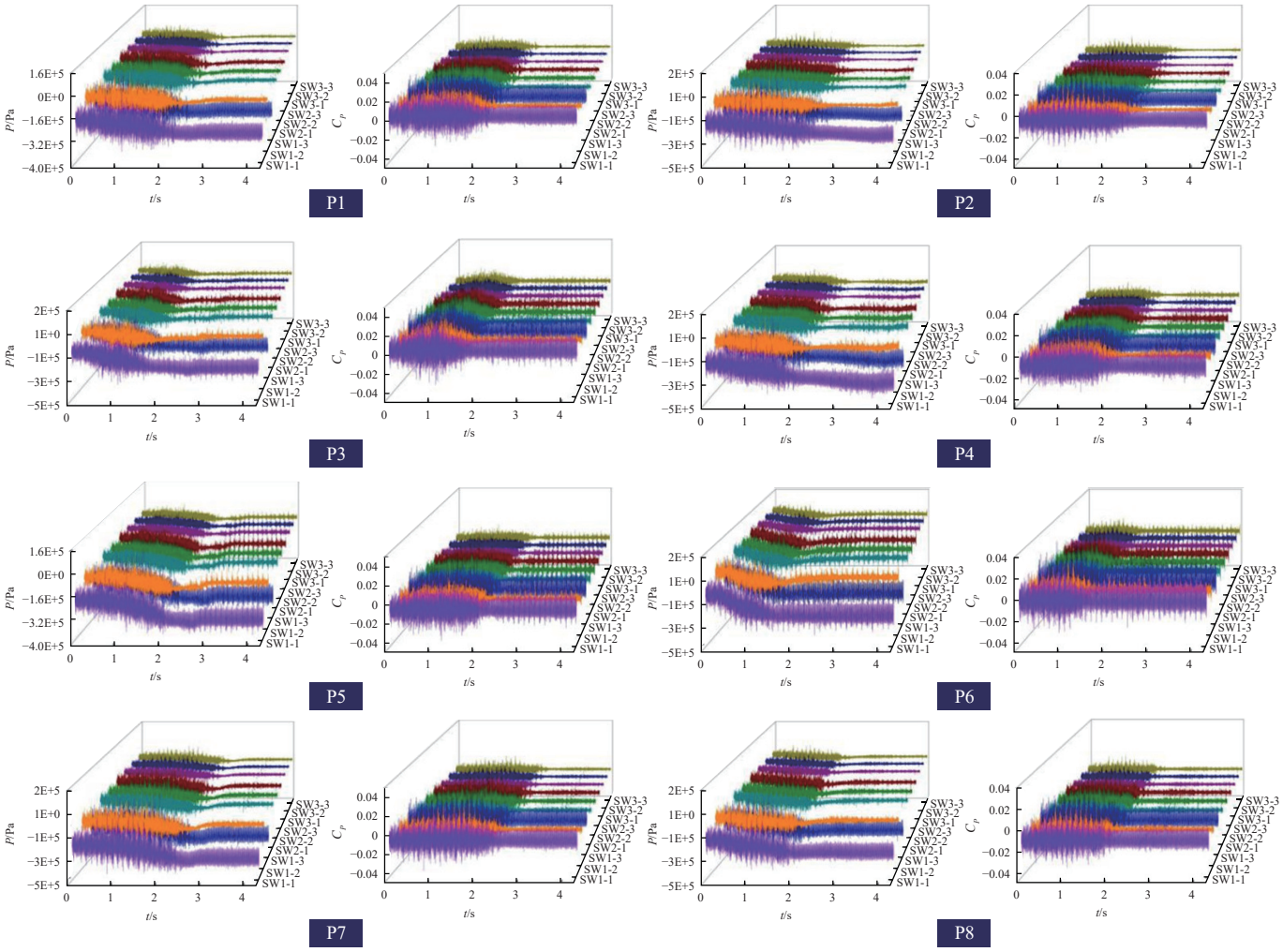

Figure 12 Frequency domain diagram of tailpipe pressure pulsation

2) Pressure pulsations during outlet pressure changes: Pressure pulsations are mainly influenced by the interference of dynamic and static components within the unit, with this interference being particularly prominent during outlet pressure changes. Regions with high-intensity pressure pulsations are primarily concentrated in the runner area, double-row blade row area, and volute area. When operating under non-optimal outlet pressure conditions, the amplitude of pressure pulsations in various flow components increases, especially in the double-row blade row area where the pressure pulsation amplitude of the moving guide vanes significantly rises. Additionally, the pressure pulsation magnitude increases more inside the volute than at the outlet.

3) Influence of outlet pressure changing rates on pressure pulsations: Faster outlet pressure changes help reduce the amplitude of pressure pulsations, especially noticeable in the interval from outlet pressure $P_{1.07\mathrm{BET}}$ to $P_{1.06\mathrm{BET}}$. In this range, faster pressure changing rates result in smaller pressure pulsation amplitudes. Under slower outlet pressure changing conditions, initially stopping the pressure change leads to the main frequency of pressure pulsations in the runner region being the same as during stable operation, both at $9f_n$. However, at this time, the pressure pulsation amplitude is smaller, and there is an increase in low-frequency, low-amplitude pulsations.

Acknowledgements

This study was supported by the Changjiang Electric Power Co., Ltd. Project (Grant No. Z232402007); "Kunlun Talents" Research Project (Grant No. 2023-QLGKLYCZX-032); Jiangsu South-to-North Water Transfer Technology Research and Development Project (Grant No. JSNSBD202303); Technology Bureau Project (Grant No. 2024-YF09-0003-GX); and Open Research Subject of Key Laboratory of Fluid and Power Machinery (Xihua University), Ministry of Education (Grant No. LTDL-2024016).

[References]

[1] Xu L C, Liu D M, Li Z, Zhao X Y, Liu X B. Experimental and numerical simulation research on flow characteristics of model pump-turbine in four-quadrant operating quadrants. Journal of Energy Storage, 2022; 54: 105083.

[2] Liu D M, Li Z, Xu L C, Li J L, Yang Y X, Wang X L, et al. Vortex motion in vaneless space and runner passage of pump-turbine in s-shaped region. Physics of Fluids, 2024; 36(2): 025115.

[3] Xu L C, Kan K, Zheng Y, Liu D M, Binama M, Xu Z, et al. Rotating stall mechanism of pump-turbine in hump region: An insight into vortex evolution. Energy, 2024; 292: 130579.

[4] Li Z G, Xu L X, Wang D, Li D Y, Li W X. Simulation analysis of energy characteristics of flow field in the transition process of pump condition outage of pump-turbine. Renewable Energy, 2023; 219: 119480.

[5] Li Z G, Li W X, Wang Q F, Xiang R, Cheng J, Han W, et al. Effects of medium fluid cavitation on fluctuation characteristics of magnetic fluid seal interface in agricultural centrifugal pump. Int J Agric & Biol Eng, 2021; 14(6): 85–92.

[6] Li W, Li Z, Han W, et al. Measured viscosity characteristics of Fe_3O_4 ferrofluid in magnetic and thermal fields. Physics of Fluids, 2023; 35(1): 012002.

[7] Chen F, Zhang J, Li Z G, Yan S N, Li W X, Yan Z Q, et al. Effect of the

surface coating of carbonyl iron particles on the dispersion stability of magnetorheological fluid. Scientific Reports, 2024; 14(1): 11358.

[8] Li W X, Li Z G, Qin Z, Yan S N, Wang Z Y, Peng S Y. Influence of the solution pH on the design of a hydro-mechanical magneto-hydraulic sealing device. Engineering Failure Analysis, 2022; 135: 106091.

[9] Walseth E C, Nielsen T K, Svingen B. Measuring the dynamic characteristics of a low specific speed pump-turbine model. Energies, 2016; 9(3): 1–12.

[10] Li X Y, Cao J W, Zhuang J L, Wu T M, Zheng H Y, Wang Y F, et al. Effect of operating head on dynamic behavior of a pump-turbine runner in turbine mode. Energies, 2022; 15(11): 4004.

[11] Li Q F, Liu M M, Zhang J X, Liu Q, Zhang Z. Analysis of flow characteristics in guide vane region of pump turbine under braking conditions. Journal of Drainage and irrigation Machinery Engineering, 2017; 35(6): 495–501. DOI: 10. 3969 /j. issn. 674-8530. 16. 0243.

[12] Kim S J, Suh J W, Yang H M, Park J, Kim J H. Internal flow phenomena of a Pump-Turbine model in turbine mode with different Thoma numbers. Renewable Energy, 2022; 184: 510–525.

[13] Yin X L, Huang X X, Zhang S Z, Bi H L, Wang Z W. Numerical investigation of flow and structural characteristics of a large high-head prototype pump-turbine during turbine start-up. Energies, 2023; 16(9): 3743.

[14] Zhang F F, Zhu D, Xiao R F, Liu W C, Tao R. Numerical investigation on the transient gas-liquid flow in the rapid switching process of pump turbine. Energy Science & Engineering, 2023; 11(8): 2710–2724.

[15] Pan S Y, Wang J, Zhao X, Ren C J, Xin Y J, Wang Z L. New design and transient flow analysis of a claw vacuum pump with novel gear-claw rotors. Vacuum, 2023; 216: 112470.

[16] Lu C S, Ding Y D, Wang H, Cheng M, Zhu X, Liao Q. Experimental study of the dynamics and mass transfer behavior of carbon dioxide bubble at different constraint limits. Chemical Engineering Science, 2024; 299: 120412.

[17] Ren Z P, Li D Y, Wang H J, Liu J T, Li Y. Computational model for predicting the dynamic dissolution and evolution behaviors of gases in liquids. Physics of Fluids, 2022; 34(10): 103310

[18] Ren Z, Li D, Hao H, et al. Gas-liquid transport behaviors and mass transfer mechanism during oxygen dissolution and evolution processes in a micropump. Journal of Fluids Engineering, 2023; 145(7): 071401.

[19] Pan S Y, Wang J, Zhao X H, Li H X, Wang Z L, Geng M F, et al. Theoretical model and simulation of a twin-Screw multiphase pump with novel smooth screw rotors for gas-oil mixed transportation. Proceedings of the Institution of Mechanical Engineers, Part A: Journal of Power and Energy, 2023; 237(6): 1251–1263.

[20] Li W X, Li Z, Han D Y S. Time-mean equation and multi-field coupling numerical method for low-Reynolds-number turbulent flow in ferrofluid. Physics of Fluids, 2023; 35(12): 125145.

[21] Liang A, Li H C, Zhang W W, Yao Z F, Zhu B S, Wang F J. Study on pressure fluctuation and rotating stall characteristics in the vaneless space of a pump-turbine in pump mode. Journal of Energy Storage, 2024; 94: 1–19.

[22] Hu L W, Liang A, Li H C, Zhang W W, Zhu B S. Impact of rotor-stator axial spacing on the gas-liquid-solid flow characteristics of a multiphase rotodynamic pump based on the Euler multi-fluid model. Physics of Fluids, 2024; 36: 1–17.

[23] Li H C, Yang J H, Zhang W W, Hu L W, Liang A, Yao Z F. Energy performance and unsteady gas-liquid flow characteristics of a multiphase rotodynamic pump: An experiment. Applied Energy, 2024; 375: 124112.

[24] Zhou W J, Ma J, Ma Z L, Yu W B, Su H H, Gao B. Fluid-structure interaction on the rotor-dynamic characteristics of a low-specific-speed centrifugal pump considering multi-scale fluid excitation effects. Physics of Fluids, 2024; 36(11): 117157.

[25] Li W X, Li Z G, Han W, Li D C, Yan S N, Zhou J P. Study of the flow characteristics of pumped media in the confined morphology of a ferrofluid pump with annular microscale constraints. Journal of Fluids Engineering, 2025; 147(2): 021201.

[26] Li W X, Li Z G, Han W, Wang Y, Zhao J L, Zhou J P. Morphologic transformation of ferrofluid during micropump driving under field control. Annals of the New York Academy of Sciences, 2025; 1543(1): 194–203.

[27] Zhou W, Jin X, Ding L, Ma J, Su H H, Zhao A. Research on vibration signal decomposition of cracked rotor-bearing system with double-disk based on CEEMDAN-CWT. Applied Acoustics, 2025; 227: 110254.

[28] Jin X, Zhou W J, Ma J, Su H H, Liu S, Gao B. Analysis on the vibration signals of a novel double-disc crack rotor-bearing system with single defect in inner race. Journal of Sound and Vibration, 2025; 595: 118729.

[29] Zhou W J, Qiu N, Wang L Q, Gao B, Liu D. Dynamic analysis of a planar multi-stage centrifugal pump rotor system based on a novel coupled model. Journal of Sound and Vibration, 2018; 434: 237–260.